Probabilistic Physics-Augmented Neural Networks for Robust Control Applied to a Slider-Crank System

Edward Kikken[a], Jeroen Willems[b], Rob Salaets[c] and Erik Hostens[d]
Flanders Make, Lommel, Belgium
fl

Keywords: Neural Networks, Physics-Augmented Neural Networks, Probablistic Neural Networks, Optimal Control, Robust Control, Physics-Informed AI, Non-Linear Dynamic Systems Modelling.

Abstract: Key industrial trends such as increasing energy and performance requirements as well as mass customization, lead to more complex non-linear machines with many variants. For such systems, variability in dynamics arising from many factors significantly affects performance. To capture this adequately we introduce a probabilistic extension of a Physics-Augmented Neural Network (PANN). We subsequently illustrate the added value of such models in robust optimal control, thereby keeping performance high while guaranteeing to meet the application's constraints. The approach is validated on a experimental slider-crank mechanism, which is ubiquitous in industrial machines.

1 INTRODUCTION

The industrial need for reduced energy consumption, increased throughput and increased production accuracy leads to ever-increasing performance requirements for mechatronic systems. These requirements result in more complex machines with e.g., input saturations, flexible behavior, highly non-linear components, many degrees of freedom (DOFs) needing to be coordinated efficiently. To further complicate matters, the current trend towards mass customization increases the number of system variants. On top of that, intrinsic fluctuations in system behavior due to e.g., changing operating temperatures, wear, friction lead to additional variability.

This increase in system complexity and variability poses challenges to model and control these systems: (i) the complex dynamics need to be accurately modelled to enable high-performance control; (ii) many models and controllers need to be developed for all the system variants; (iii) models need to capture the intrinsic variability; and (iv) controllers need to be stable and performant not only for the nominal dynamics, but for the full range of variability, without resulting in unnecessary conservative and sub-optimal control.

[a] https://orcid.org/0000-0002-5769-5814
[b] https://orcid.org/0000-0002-2727-6096
[c] https://orcid.org/0000-0002-4835-0793
[d] https://orcid.org/0000-0003-2482-7523

In industry, models targeted for model-based optimal control are derived from physical knowledge. However, with ever-increasing system complexity and variability this is becoming more-and-more labor intensive and requires more-and-more expert knowledge. The alternative approach is to build data-driven models. The methods for classical system identification have been around for a long time (Ljung, 1998) and are usually employed for linear or linearized systems. These methods have also been extended for nonlinear system identification with great effect, but often require specialized numerical procedures (Schoukens and Ljung, 2019). The success of Machine Learning (ML) techniques as generic non-linear modelling tools has motivated to use algorithms such as neural networks (NNs) in a Nonlinear Finite Impulse Response (NFIR) setup or recurrent neural networks (RNNs). They can be used to fit dynamic systems using limited expert knowledge (Forgione and Piga., 2020; Chen et al., 2019; De Groote et al., 2021a; Beintema et al., 2021). Furthermore, auto-differentiation as supported by frameworks such as Pytorch (Paszke et al., 2019) and Tensorflow (Abadi et al., 2015) has enabled significant computational speed-up of nonlinear system identification. However, purely data-driven approaches have some downsides compared to physical modelling: they require more data since they have more parameters, they extrapolate poorly outside of the operating domain covered by the training data, and interpretability of parameters is lost.

Kikken, E., Willems, J., Salaets, R. and Hostens, E.
Probabilistic Physics-Augmented Neural Networks for Robust Control Applied to a Slider-Crank System.
DOI: 10.5220/0012168200003543
In *Proceedings of the 20th International Conference on Informatics in Control, Automation and Robotics (ICINCO 2023) - Volume 1*, pages 152-161
ISBN: 978-989-758-670-5; ISSN: 2184-2809

To find a middle ground between these two approaches, various approaches have been researched. They can be organized into two main categories (Karniadakis et al., 2021):

- Physics-Inspired Neural Networks (PINNs) start from a neural network and enforce physical laws in the loss function of the NN (Yang et al., 2021; Raissi et al., 2019; Schiassi et al., 2021);
- Physics-Augmented Neural Networks (PANNs) start with a physical model, and augment it with NNs in its dynamic equations (De Groote et al., 2021a; De Groote et al., 2021b).

In this work we will extend PANNs by not only modelling the nominal deterministic behavior of a dynamic system, but also its variability and uncertainty. To do so, we will use the concept of a Probabilistic Neural Net (PNN) (Streit and Luginbuhl, 1994; Bishop, 1994; Lakshminarayanan et al., 2017). Modeling probability distributions with NNs is common practice, and its pitfalls are well known (Seitzer et al., 2022; Bishop, 1994). PNNs do not only capture aleatoric uncertainty on the predicted outputs, but also cover the model bias if present. Strongly linked with uncertainty modelling are methods that estimate the epistemic uncertainty, as represented by the parameter uncertainty, such as Bayesian Neural Networks (Goan and Fookes, 2020), Monte-Carlo Dropout (Gal and Ghahramani, 2016) or Gaussian Stochastic Weight Averaging (Morimoto et al., 2022). These works complement the techniques in this paper, but we leave epistemic uncertainty out of this analysis. We assume here that sufficient data is available such that the epistemic uncertainty is negligible as compared to the aleatoric uncertainty.

To control complex non-linear systems one must move away from classical control approaches (e.g., PID, simple model-based or ad hoc engineered feedforward) towards more powerful model-based optimization-based techniques. Such methods can deal with constraints, use preview, handle complex and non-linear behavior and coordinate multiple DOFs (Forbes et al., 2015), by exploiting the prediction capabilities of dynamic models such as PANNs, see for example (Salzmann et al., 2022; Spielberg et al., 2022; Kikken et al., 2022). We have extended these approaches to also include uncertainty, resulting in a robust controller, inspired by the robust optimal control problem (OCP) for physical models developed in (Willems et al., 2018).

To experimentally validate the approach, it has been applied to a slider-crank setup that converts the rotary movement of a motor into a linear movement. Such mechanisms are ubiquitous in industry, e.g., weaving looms, piston compressors, etc. We will assume some initial physical relations of the setup are known (e.g., kinematics, some physical parameters), but all missing dynamics will be automatically found using the PPANN techniques.

The remainder of this paper is organized as follows. Section 2 introduces the proposed methodology. We discuss the structure of a physics-augmented neural network and extend it to our probabilistic variant. Next, we detail the formulation of the optimal control problem and how it is extended to exploit the PPANN's uncertainty to find a robust solution. Section 3 introduces the slider-crank setup on which the developed algorithms are experimentally validated. We explain how we generated a dataset on this setup, on which we have trained the PPANN that is subsequently used to solve the robust optimal control problem. This OCP solution is experimentally validated thereby demonstrating the advantage of the proposed approach. Finally, we formulate our conclusions and future work in Section 4.

2 METHODOLOGY

2.1 Notation

We consider a (non-)linear dynamic model in the form of a set of ordinary differential equations (ODE) represented in state-space, i.e., explicit format (see Eq. 1a), or implicit format (see Eq. 1b). These continuous-time models are given in the form of:

$$\hat{\dot{x}}(t) = f(x(t), u(t), p), \tag{1a}$$

$$0 = f(x(t), u(t), p), \tag{1b}$$

where $x \in \mathbb{R}^{n_x}$ and $\hat{x} \in \mathbb{R}^{n_x}$ denote the *measured* and (when applicable) *model-predicted* state variables respectively (different for the two ODE variants), $u \in \mathbb{R}^{n_u}$ the inputs, $p \in \mathbb{R}^{n_p}$ the model parameters and function f denotes the ODE function. For the considered class of models, we assume all states are observable, so an output function is omitted.

When sampling time t, we denote a specific time instant as t_k with $k \in [1, N]$, with N the number of time samples. For notational compactness we will denote any time dependent signal $y(t)$, sampled at time instant k, as y_k (and similar for e.g., u_k, x_k, $\dot{x}_k$).

2.2 Combining Data-Driven and Physical Modelling

In this section, we will first describe the architecture of the combined physical equations and neural networks (PANN) and the used approach for training. Secondly, we will extend the PANN towards the proposed probabilistic modelling and training approach (PPANN).

2.2.1 Physics-Augmented Neural Networks

A PANN integrates a (or multiple) neural network(s) into physical equations. These physical equations are expressed as an explicit ODE based on lumped physical parameters p_{phys}. A PANN's function f contains the physical equations but also a neural network that captures unmodelled phenomena z that depend on states and/or control inputs e.g., a state dependent load, complex friction or efficiency maps. For these effects no analytical expression has been derived and they cannot be experimentally measured directly. Note that the inputs to the neural network are often normalized, scaled or passed through some engineered static function, which we will denote with g. The above results in the following general dynamic equation that is considered throughout this paper where neural network parameters (i.e., weights and biases) p_{NN} and physical parameters p_{phys} need to be identified:

$$\hat{\dot{x}}(t) = f(x(t), u(t), z(g(x(t), u(t)), p_{NN}), p_{phys}). \quad (2)$$

For notational convenience we will often write Eq. 2 in the simplified and time-sampled form:

$$\hat{\dot{x}}_k = f(x_k, u_k, z_k, p), \quad (3)$$

where p denotes the combination of p_{NN} and p_{phys}. The derivative function of the PANN can then be propagated forward in time using Euler's method to get the state propagation in discrete-time:

$$\hat{x}_{k+1} = f(x_k, u_k, z_k, p)\Delta t + x_k, \quad (4)$$

where Δt denotes the time step of the forward Euler time integration and $\hat{x}_{k+1}$ the model-predicted new state. Other time-integration schemes can also be used of course. The PANN is graphically depicted in Fig. 1.

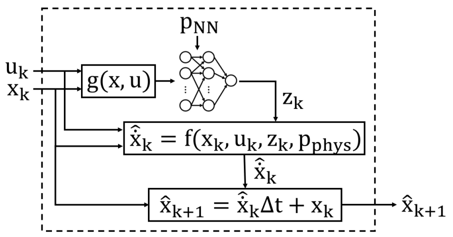

p_NN
u_k
x_k
g(x, u)
z_k
$\hat{\dot{x}}_k = f(x_k, u_k, z_k, p_{phys})$
$\hat{\dot{x}}_k$
$\hat{x}_{k+1} = \hat{\dot{x}}_k \Delta t + x_k$
$\hat{x}_{k+1}$

Figure 1: The explicit PANN model structure with time integrator.

To fit the model to the measurement data we minimize the error between the model-predicted state $\hat{x}$ and the measured state x:

$$\underset{p}{\text{minimize}} \qquad \frac{1}{N}\sum_{k=1}^{N}(x_k - \hat{x}_k)^2 \quad (5)$$

The advantage of training an explicit ODE (or PANN) using time-integration is that, when states are predicted forward in time multiple steps, so-called N-step ahead prediction (De Groote et al., 2021a), the optimization becomes less sensitive to measurement noise.

Another way of formulating the dynamics of the PANN is the implicit ODE format: a function such as a force or torque balance that should equal zero:

$$0 = f(x_k, u_k, z_k, p). \quad (6)$$

When the measured states x and control inputs u are entered into this function, the parameters p can be optimized to minimize its left hand side, i.e., residual r_k at each time step k:

$$\underset{p}{\text{minimize}} \qquad \frac{1}{N}\sum_{k=1}^{N} r_k^2. \quad (7)$$

Note that this way of fitting the model does not require a time-integrator. However, it is more sensitive to noise than N-step ahead prediction fitting, also because the measurement x needs to contain higher derivatives (e.g., acceleration), which are harder to measure (or estimate from measurements) accurately and will typically exhibit greater noise levels.

2.2.2 Probabilistic Physics-Augmented Neural Networks

In this section we will integrate the concepts of a PNN and a PANN to find the novel probabilistic physics-augmented neural network (PPANN).

A PNN is a neural network architecture that replaces a deterministic mapping of its input $g(x,u)$ to output z with a parameterized probability distribution of z. In our case we choose a normal distribution which means that the PNN outputs are the mean z^{μ} and standard deviation z^{σ}, see Fig. 2.

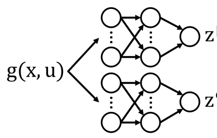

Figure 2: The PNN neural network architecture.

We want to train a PNN that matches the measured data and its variability as accurately as possible. This means we want to maximize the likelihood of the model predictions explaining the observed data. This can be achieved using a negative log likelihood (NLL) (Lakshminarayanan et al., 2017) cost function to train the parameters p_{NN} in the PNN. We assume that the observed variability can be captured in a Gaussian (i.e., normal) distribution, so we can use the following expression for the NLL cost:

$$\underset{p_{NN}}{\text{minimize}} \; \frac{1}{2N}\sum_{k=1}^{N}\left(\frac{(z_k - z_k^{\mu})^2}{z_k^{\sigma 2}} + \log((z_k^{\sigma})^2)\right), \quad (8)$$

where z_k denotes the measured output that is captured by the PNN.

Interconnecting the PNN and the PANN is rather straightforward and depicted in Fig. 3. However, we

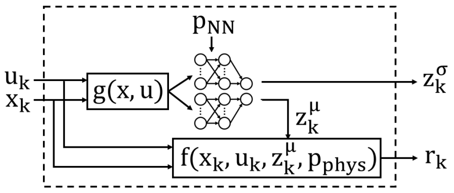

Figure 3: The implicit PPANN model structure.

want to predict z^μ and z^σ using the data we measure on the complete system: we do not have a direct measurement z_k. To resolve this, we must propagate z^μ and z^σ of the neural network to the PPANN residual output r, which results in the following modified NLL optimization to train PPANN's:

$$\underset{p}{\text{minimize}}\ \frac{1}{2N}\sum_{k=1}^{N}\left(\frac{r_k^2}{(\frac{dr_k}{dz_k^\mu}z_k^\sigma)^2}+\log(\frac{dr_k}{dz_k^\mu}z_k^\sigma)^2)\right). \quad (9)$$

This cost function can easily be extended when multiple PNN are inserted into the PANN.

There are however two drawbacks related to training the PPANN using the cost described in Eq. 9. The first is related to our earlier remark that with the implicit formulation we cannot use the N-step ahead prediction for training. Secondly, there is a risk that the optimization gets stuck in a local optimum where the mean model z^μ fits poorly which is compensated with a large z^σ to explain the measured data. Yet, although we can easily propagate z^μ N steps ahead in time through the explicit ODE, the same cannot be done as straightforwardly for z^σ. Therefore, to ensure we get an accurate mean prediction and limit the model bias, but in the same time still allow for the probabilistic extension, we split the training approach in two phases:

1. Train the mean neural network z^μ of the PPANN using N-step ahead prediction with a MSE cost function. Note that the MSE cost is equivalent to assuming z^σ is constant, therefore z^σ will not run away to compensate for a poor z^μ fit.
2. Fix z^μ and train the sigma network z^σ of the PPANN using the NLL cost from Eq. 9.

2.3 Optimal Control

The formulation of a generic discrete-time optimal control problem is:

$$\underset{x,u}{\text{minimize}}\quad \mathcal{J}_{\text{OCP}}(x,u) \quad (10a)$$

$$\text{s. t.}\quad x_{k+1}=f(x_k,u_k,z_k,p)\Delta t+x_k,\ \ \forall\ k\in[1,N] \quad (10b)$$

$$\underline{h}\le h(x,u)\le \bar{h}. \quad (10c)$$

In the above, Eq. 10a denotes the cost function which can depend on states and/or inputs, Eq. 10b implements the model dynamics using a multiple shooting approach, see (Bock and Plitt, 1984) for more details. Finally, Eq. 10c implements the desired constraints h (e.g., initial condition, input and path constraints) lower and upper bounded by $\underline{h}$ and $\bar{h}$.

The resulting discrete-time optimization problem is a large-but-sparse non-linear program (NLP), containing continuous optimization variables. We will use the CasADi framework (Andersson et al., 2019) to efficiently set-up the problem, which employs algorithmic differentiation, and we will solve it using the gradient-based interior point optimization algorithm IPOPT (Wächter and Biegler, 2006).

2.4 Robust Optimal Control Using Probabilistic Physics-Augmented Neural Networks

In this section, we will describe the extension of the optimal control problem of Section 2.3 to a robust OCP leveraging the dynamics captured in the PPANN.

As shown in the previous section, we can embed state-space model dynamics, for example of a PANN or PPANN, in the optimization problem. Ideally one would also add the PPANN's description of uncertainty to the OCP to formulate constraints with respect to the uncertain dynamics. However, since there is no explicit formulation for the propagation of uncertainty in time this can not be done. Instead, we will compute the uncertainty in time by, at each time step k, Monte Carlo sampling j times the distribution fitted by the PPANN to get $z_k^{(j)}$ and performing the time integration of the dynamics for each k and j as:

$$\hat{x}_{k+1}^{(j)}=f(x_k,u_k,z_k^{(j)},p)\Delta t+x_k, \quad (11)$$

If we stack these varying state propagations into $\hat{x}^{\text{MC}}$, we can once again compute a standard deviation $\sigma(\hat{x}^{\text{MC}})$. This can then be used to compute the 3σ upper and lower bound of the states. These bounds can be used to add a robustness safety margin to the state constraint (Eq. 10c) after which the OCP can be solved again with the updated constraints.

3 EXPERIMENTAL RESULTS

In this section, we explain the approach proposed in Section 2 applied to a lab-scale slider-crank mechanism designed to mimic weaving looms and similar industrial systems. First, we introduce the setup and generate a dataset. Secondly, we train the PPANN on the dataset and lastly, we solve a robust optimal control problem and validate its performance on the setup.

3.1 Slider-Crank Mechanism

We consider the control of a slider-crank mechanism, which is shown schematically in Fig. 4. The mechanism converts a rotary motion $\theta \in \mathbb{R}$ into a linear displacement $x^{\text{slider}} \in \mathbb{R}$ using input torque $\tau \in \mathbb{R}$ - a motion conversion that often emerges in industrial applications, such as weaving looms, compressors and piston engines. The system contains non-linearities and has dead points. The state vector of the system is defined as $x = \begin{bmatrix}\theta & \omega\end{bmatrix}^T$, with angular velocity $\omega = \dot{\theta}$ and input $u = \tau$.

The slider displacement x^{slider} is calculated using a straightforward kinematic function that is assumed to be known: $x^{\text{slider}} = l_1 cos(\theta) + l_2 cos(\phi) + l_1 - l_2$, employing geometric constraint $\phi = sin^{-1}(\frac{l_1}{l_2} sin(\theta))$. The crank-arm length l_1 = 0.05 m and connecting-rod length is set to l_2 = 0.3 m respectively. Furthermore, we have approximate values for inertia ($J_m = 3e^{-3}$ kg/m^2), damping (B_m = 0.1 Ns/rad) and the stiffness (K_m = 1 N/rad).

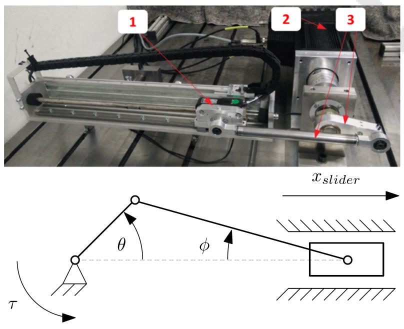

Figure 4: Picture and schematic overview of the slider-crank system consisting of: (1) linear slider, (2) rotary motor and (3) the crank and connecting rod.

3.2 Dataset Generation

We sample the measurements at 500 Hz ($\Delta t = \frac{1}{500}$ s) and generate 90 seconds of data. In order to excite the system, we have generated a semi-random input torque (which is filtered by a low-pass filter), as shown in the top plot of Fig. 5. Furthermore, to increase the variability of the system and better validate our method, we have applied a white-noise input force on the slider with a peak amplitude of 30 N (which acts as a *non-measured* disturbance). Applying these inputs results in the measured state evolution as shown in Fig. 5.

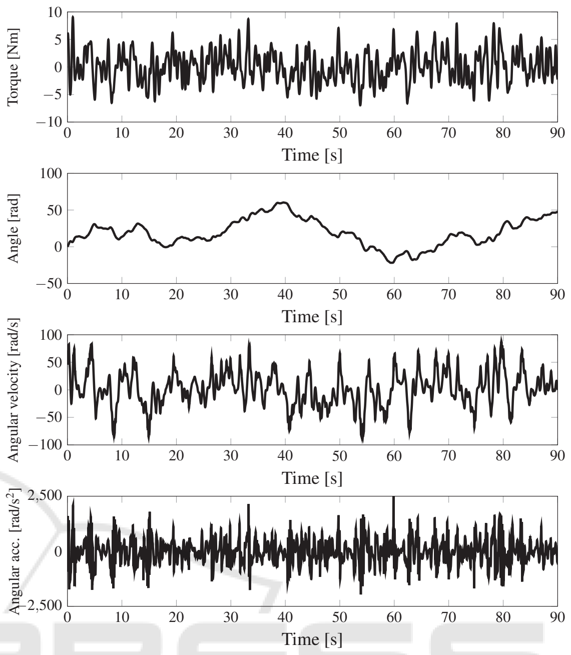

Figure 5: The input torque considered to excite the physical system and the measured states of the physical model after excitation with the given input torque.

In Fig. 6, the coverage maps are shown for the entire dataset. It can be seen that the maps are quite densely populated, i.e., the training data is quite rich (within the considered bounds that are chosen large enough to ensure that the OCP solution falls within them), which is required for an accurate fit of the PPANN. Note that the angles are plotted between 0 and 2π, since it is assumed that the system is periodic over each rotation.

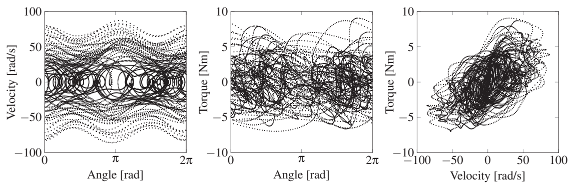

Figure 6: The coverage maps of the dataset.

3.3 PPANN Design and Training

In this section, we will discuss the architecture of the PPANN model for the considered slider-crank system and then execute the training, using the dataset created in the previous section.

3.3.1 Parameterization of the Considered PPANN

The state propagation function of the considered PPANN (explicit form) is given as follows:

$$\hat{x}_k = f(x_k, u_k, z_k, p) = \begin{bmatrix} \omega_k \\ \hat{\alpha}(x_k, u_k, z_k, p) \end{bmatrix}. \quad (12)$$

We exploit the fact that for the given system, $\dot{\theta} = \omega$, i.e., the derivative of the first state is equal to the second state. Therefore, it is not needed to have the PPANN predict both states, we will instead let it predict the derivative of the second state, i.e., $\hat{\alpha} = \hat{\dot{\omega}}$. As a result, the relation between θ and ω remains maintained even in case of an imperfect model.

In the above, function g denotes the mapping from state and input to the inputs of the PPANN. Instead of using the states of the slider crank system (and its input) directly as input, i.e., $\begin{bmatrix}\theta & \omega & \tau\end{bmatrix}^T \in \mathbb{R}^3$, we use: $g(x,u) = \begin{bmatrix}\sin(\theta) & \cos(\theta) & \omega & \tau\end{bmatrix}^T \in \mathbb{R}^4$, thereby constraining the input space of the neural networks. It is equivalent to imposing a 2π periodicity over the angle θ.

In order to derive function $\hat{\alpha}$, we first employ a simple and generic 2nd order linear system:

$$\hat{\alpha}_{lin}(x_k, u_k, p_{phys}) = \frac{\tau_k - B_m\omega_k - K_m\theta_k^{mod}}{J_m}. \quad (13)$$

In the above, $p_{phys} = \begin{bmatrix}J_m & B_m & K_m\end{bmatrix}$, and θ^{mod} is equal to θ modulo 2π. Second, the above linear model is augmented to a PPANN (yielding $\hat{\alpha}$ from Eq. 12), by employing three neural networks $z^{\mu J}$, $z^{\mu B}$ and $z^{\mu K}$:

$$\hat{\alpha}(x_k, u_k, z_k, p) = \frac{\tau_k - B_m(1+z_k^{\mu B})\omega_k - K_m(1+z_k^{\mu K})\theta_k^{mod}}{J_m(1+z_k^{\mu J})}. \quad (14)$$

In the above, three separate neural networks are present, the mean inertia network output $z^{\mu J}$, mean damping network $z^{\mu B}$ and mean stiffness network $z^{\mu K}$, which allow the additional (non-)linear dynamics to be modelled as well. Note that networks $z^{\mu J}$ and $z^{\mu K}$ are parameterized to be a function of only (the transformed) θ, i.e., $\begin{bmatrix}\sin(\theta) & \cos(\theta)\end{bmatrix}^T$, thereby allowing for a position-dependent inertia and stiffness profile. $z^{\mu B}$ is parameterized to be a function of both (the transformed) θ and ω, i.e., $\begin{bmatrix}\sin(\theta) & \cos(\theta) & \omega\end{bmatrix}^T$, allowing not only position dependency to be accounted for, but also speed-dependent effects (e.g., Stribeck friction).

For the z^{μ} networks of the PPANN, each is constructed using a single hidden layer of 100 neurons, which is shown to be able to to approximate any continuous function (Hornik et al., 1989). We have used a linear activation function for the final layer (the output layer), and tanh activations for the previous layers. For the z^{σ} networks, each of the three uses 10 neurons.

3.3.2 Training the PPANN

Now that the architecture has been defined, we will use the dataset obtained in Section 3.2 to train the neural networks. We use the first 87 seconds for training, and the last 3 seconds for validation. A learning rate of $5e^{-3}$ is used for the Adam optimizer (Kingma and Ba, 2014). As described in Section 2.2.2, we first train the z^{μ} part of the PPANN (using cost function given by Eq. 5 and N-step ahead training with a prediction horizon of $N_s = 10$) and afterwards, the z^{σ} part of the PPANN is trained (employing Eq. 9).

The resulting 3-D maps for each of the six networks trained are shown in Fig. 7. We make the following observations:

- For the inertia maps (top row), oscillatory behavior can be seen for the $z^{\mu J}$ network: the inertia varies as a function of the angle, due to the kinematic relation between motor rotation and slider translation. When the crank and connecting rod are parallel to each other ($\theta = \{0, \pi, 2\pi\}$), the perceived inertia is the lowest (dead points), and highest at ($\theta = \{\frac{1}{2}\pi, 1\frac{1}{2}\pi\}$). The uncertainty is the highest when the crank and rocker are in the upper position (between 0 and π), but compared to the other networks it is small.
- For the damping maps (middle row), again and varying behavior can be seen as a function of angle and velocity. The damping seems to be the highest around low speeds, when the crank and rod are approximately perpendicular (e.g., due to stick-slip friction present on the slider), and again increases for higher speeds (viscous friction in the rotary motor).
- For the spring maps (bottom row), it can be seen that the μ network oscillates around -1. Since this thus almost cancels out the stiffness related term ($K_m(1+z_k^{\mu K})\theta_k^{mod}$), in Eq. 14, the contribution of stiffness to the total torque is thus rather limited. The remaining part can for example be attributed to effects such as cogging and flexibility of the setup. The uncertainty is the highest when the crank and rocker are in the upper position (between 0 and π).

In Fig. 8, the output of the z^{μ} part of the trained PPANN (deterministic part) is shown for the entire validation dataset. It can be seen that a good match is obtained between the validation data and the prediction of the neural network, even for longer prediction horizons (in this case: 3 seconds). The observed mismatch can be attributed to variability in the behavior, such as (non-measured) white noise force excited by the linear

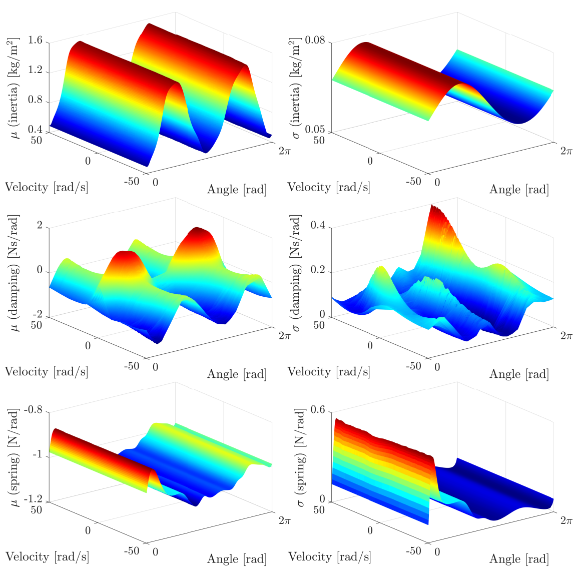

Figure 7: Resulting 3-D maps for the μ and σ networks.

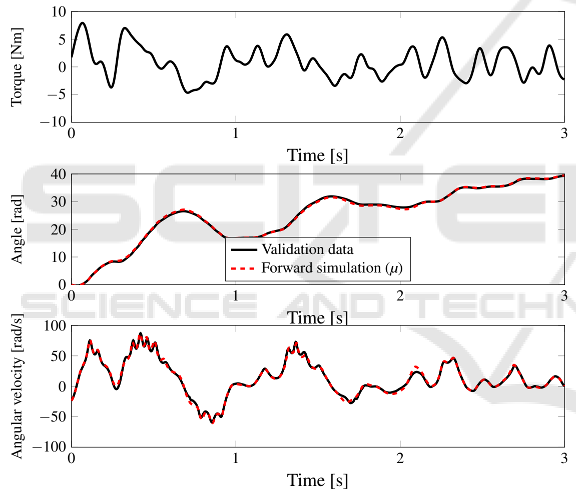

Figure 8: The results of the trained PPANN demonstrated on the validation dataset.

motor acting on the slider, as well as backlash in the setup.

Next, we demonstrate the uncertainty part captured by the trained PPANN, by including the (stochastic) z^{σ} nets as well in the simulation. To do so, we have employed Monte Carlo sampling (see Eq. 11); sampling the trained model 100 times (yielding $\hat{x}^{(j)}$ with $j = 1, \ldots, 100$). In this way we obtain a varying state propagation, on which we can compute the standard deviation at each time step, similar to as discussed in Section 2.4, allowing to compute the 3σ upper and lower bounds. The results are shown in Fig. 9. We have shown the original validation data and forward simulation of the deterministic part (μ), as well as the $\underline{x}$ and $\bar{x}$ bounds: forming a state and time-propagation dependent uncertainty band around the deterministic part.

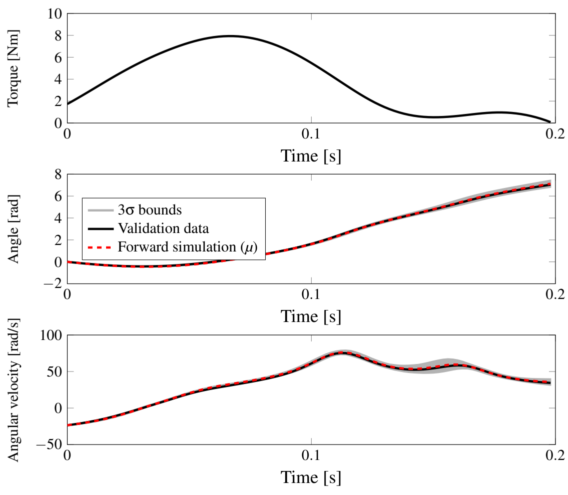

Figure 9: Uncertainty simulation on part of validation dataset.

3.4 Optimal Control and Results

In this section, we will solve a typical control case for such an oscillating mechanism using the robust OCP approach described in Sections 2.3 and 2.4. We use the trained PPANN, and validate the results by running it multiple times on the physical setup to verify if the solution indeed performs robustly.

3.4.1 Problem Formulation

First, we will solve an optimal control problem that minimizes the input torque, while meeting several constraints on the states. We set up the optimal control problem denoted in Eq. 10, with cost function $\mathcal{J}_{\text{OCP}} = \sum_{k=1}^{N} u_k^2 + 1e^{-4} \sum_{k=1}^{N-1} (\frac{\Delta u_k}{T_s})^2$, where Δ denotes the discrete derivative operator. We set the horizon length N to 150 samples, and use a sampling time of $\frac{1}{500}$ s. Additionally, the following motion constraints are taken into account:

$$\begin{cases} x_k^{\text{slider}} \geq 0.08, & k \in \{50, 100\}, \\ \theta_1 = \pi, & \omega_1 = 0, \\ \theta_N = 3\pi, & \omega_N = 0. \end{cases} \tag{15}$$

The first constraint involves the height (0.08 m) and timing (samples 50 and 100) of the displacement of the slider. The second and third constraint denote the initial and final angular conditions.

3.4.2 Step 1: Solve non-Robust OCP (Without Uncertainty)

Using the model trained in the previous section, we have solved the OCP. The results are shown in Fig. 10.

The top plot shows the calculated input torque, and the bottom plot shows the slider displacement calculated using the mean PPANN, as well as the given constraint surface. It can be seen that the nominal OCP result (calculated on the mean PPANN) satisfies the given constraints.

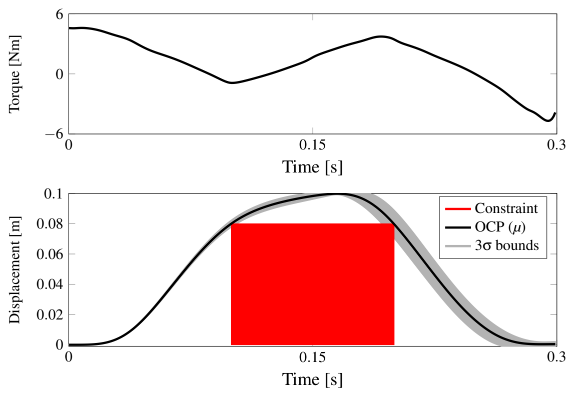

Figure 10: OCP results (non-robust case) solved using the mean PPANN. The 3σ bounds are computed and shown afterwards.

3.4.3 Step 2: Determine Uncertainty (Given OCP Solution)

Next, the 3σ standard deviation on the slider displacement, denoted by $3\sigma(x_k^{\text{slider, MC}})$, is calculated by Monte Carlo sampling the PPANN with variability (using 100 trajectories, see Eq. 11). In Fig. 10, it can be seen that if uncertainty is accounted for, satisfaction of the constraints is not guaranteed.

3.4.4 Step 3: Solve Robust OCP (Accounting for Uncertainty)

In this step, the goal is to solve a robust OCP, i.e., an OCP which guarantees constraint satisfaction given the modelled uncertainty. To do so, we update the constraints on the slider displacement (see Eq. 15) to:

$$x_k^{\text{slider}} - 3\sigma(x_k^{\text{slider, MC}}) \geq 0.08, \;\; k \in \{50, 100\}. \quad (16)$$

Note that only the lower bound −3σ case is considered, since it is the only active constraint. The results are shown in Fig. 11. The top plot shows the (previously computed) non-robust and robust input torque, which does account for the uncertainty. The bottom plot shows the resulting slider displacement calculated using the robust OCP and its 3σ bounds, again computed using Monte Carlo simulation. In the figure, it can be seen that the updated result is indeed feasible, given the (re-computed) uncertainty. Note that for this example we were able to obtain a robust solution by solving the OCP twice (once for the nominal case and once for the case accounting for uncertainty). Note that multiple iterations could be considered in case the uncertainty would change more between operating regions.

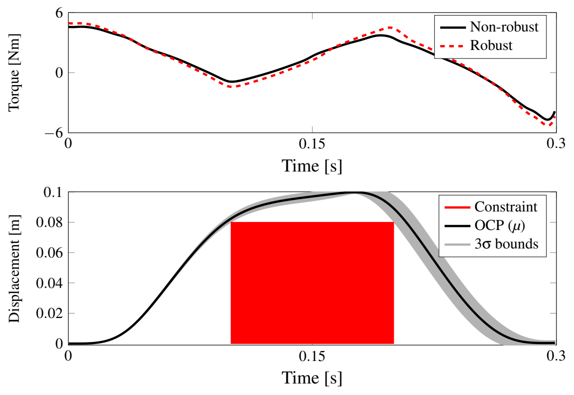

Figure 11: OCP results (robust case), accounting for uncertainty.

3.5 Implementation on Physical Setup

In this section, we will implement the OCP results determined in the previous section on the physical setup, to validate the approach presented in this paper. We have applied both the input signals computed in the previous section (non-robust and robust case) 100 times each. In Fig. 12 the results are shown: the constraint box, the slider displacement computed by the OCP in simulation, the mean displacement measured on the experimental setup and the corresponding 3σ bounds (calculated on the experimental data). The top plot shows the result for the non-robust case. Similar to as shown in simulation, if uncertainty is not accounted for, the constraints can be violated. The bottom plot shows the robust case, where uncertainty is accounted for. In this case, it can be seen that the constraints are indeed satisfied. Note that however the 3σ band seems to be smaller for the experimental case compared to the simulation case (see Fig. 11). This could be attributed to for example imperfections (bias) in the training of the μ network, or reduced heating up of the setup (thereby changing the friction), compared to the longer duration training data.

4 CONCLUSIONS

In this work we demonstrated an approach to augment a physical model with probabilistic neural networks to capture unmodelled effects. It predicts not only the mean system behavior but also its variance. We coined this novel model structure PPANN. Prediction of the mean and variance was exploited using a robust optimal control approach, where the predicted vari-

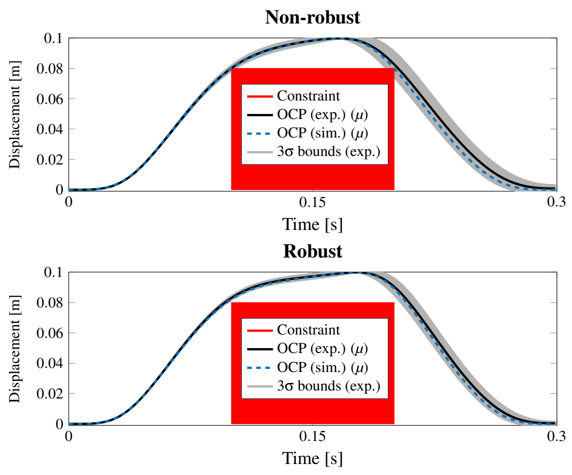

Figure 12: Results of the experimental validation, for both the non-robust and robust case.

ability was included in the control optimization constraints to ensure the necessary robustness. Validation of the PPANN model and the robust optimal control approach was performed on a slider-crank setup mimicking an industrial weaving loom. It was shown that the PPANN captured the mean system behavior, but also its variability, as intended. Furthermore, the robust controller was shown to have (near-)minimal but sufficient robustness. The constraints were satisfied whilst achieving high performance thereby validating the approach on a real system.

Future work will look into the following topics:

- Research how to meaningfully propagate uncertainty in time and train both model mean and variance using N-step ahead predictions. This will also allow us to directly include variability in the robust OCP and remove the need for iterative OCP solving.
- Train the PPANN in a single shot, as opposed to the current two-phase approach, whilst finding the minimal uncertainty.
- Research into training physical and neural parameters at the same time, whilst maximizing the contribution of physical parameters (which have the advantage of extrapolation beyond the trained region).
- Add uncertainty to the physical parameters in case there is reason to assume these are probabilistic.
- Applying the current (off-line) optimal control problem in an (on-line) model-predictive control setting.

ACKNOWLEDGMENTS

This work has been carried out within the framework of Flanders Make's IRVA project HAIEM (Hybrid AI for Estimation in Mechatronics), funded by Flanders Make and the AI Research Program of the Flemish Government. Flanders Make is the Flemish strategic research centre for the manufacturing industry.

REFERENCES

Abadi, M., Agarwal, A., Barham, P., Brevdo, E., Chen, Z., Citro, C., Corrado, G. S., Davis, A., Dean, J., Devin, M., Ghemawat, S., Goodfellow, I., Harp, A., Irving, G., Isard, M., Jia, Y., Jozefowicz, R., Kaiser, L., Kudlur, M., Levenberg, J., Mané, D., Monga, R., Moore, S., Murray, D., Olah, C., Schuster, M., Shlens, J., Steiner, B., Sutskever, I., Talwar, K., Tucker, P., Vanhoucke, V., Vasudevan, V., Viégas, F., Vinyals, O., Warden, P., Wattenberg, M., Wicke, M., Yu, Y., and Zheng, X. (2015). TensorFlow: Large-scale machine learning on heterogeneous systems. Software available from tensorflow.org.

Andersson, J. A. E., Gillis, J., Horn, G., Rawlings, J. B., and Diehl, M. (2019). CasADi – A software framework for nonlinear optimization and optimal control. *Mathematical Programming Computation*, 11(1):1–36.

Beintema, G., Toth, R., and Schoukens, M. (2021). Nonlinear state-space identification using deep encoder networks. In *Learning for dynamics and control*, pages 241–250. PMLR.

Bishop, C. (1994). Mixture density networks. Workingpaper, Aston University.

Bock, H. G. and Plitt, K.-J. (1984). A multiple shooting algorithm for direct solution of optimal control problems. *IFAC Proceedings Volumes*, 17(2):1603–1608.

Chen, R. T. Q., Rubanova, Y., Bettencourt, J., and Duvenaud, D. (2019). Neural ordinary differential equations. *arXiv preprint arXiv:1806.07366*.

De Groote, W., Kikken, E., Hostens, E., Van Hoecke, S., and Crevecoeur, G. (2021a). Neural network augmented physics models for systems with partially unknown dynamics: application to slider–crank mechanism. *IEEE/ASME Transactions on Mechatronics*, 27(1):103–114.

De Groote, W., Van Hoecke, S., and Crevecoeur, G. (2021b). Physics-based neural network models for prediction of cam-follower dynamics beyond nominal operations. *IEEE/ASME Transactions on Mechatronics*, 27(4):2345–2355.

Forbes, M. G., Patwardhan, R. S., Hamadah, H., and Gopaluni, R. B. (2015). Model predictive control in industry: Challenges and opportunities. *IFAC-PapersOnLine*, 48(8):531–538.

Forgione, M. and Piga., D. (2020). Model structures and fitting criteria for system identification with neural networks. *2020 IEEE 14th International Conference* *on Application of Information and Communication Technologies (AICT), pages 1–6. IEEE, 2020.*

Gal, Y. and Ghahramani, Z. (2016). Dropout as a bayesian approximation: Representing model uncertainty in deep learning.

Goan, E. and Fookes, C. (2020). Bayesian neural networks: An introduction and survey. In *Case Studies in Applied Bayesian Data Science*, pages 45–87. Springer International Publishing.

Hornik, K., Stinchcombe, M., and White, H. (1989). Multilayer feedforward networks are universal approximators. *Neural networks*, 2(5):359–366.

Karniadakis, G., Kevrekidis, Y., Lu, L., Perdikaris, P., Wang, S., and Yang, L. (2021). Physics-informed machine learning. *Nature Reviews Physics*, 3:422–440.

Kikken, E., Depraetere, B., and Willems, J. (2022). Bridging dynamic neural networks and optimal control. In *41st Benelux Meeting on Systems and Control*, Brussels, Belgium.

Kingma, D. P. and Ba, J. (2014). Adam: A method for stochastic optimization. *arXiv preprint arXiv:1412.6980.*

Lakshminarayanan, B., Pritzel, A., and Blundell, C. (2017). Simple and scalable predictive uncertainty estimation using deep ensembles.

Ljung, L. (1998). *System Identification*, pages 163–173. Birkhäuser Boston, Boston, MA.

Morimoto, M., Fukami, K., Maulik, R., Vinuesa, R., and Fukagata, K. (2022). Assessments of epistemic uncertainty using gaussian stochastic weight averaging for fluid-flow regression. *Physica D: Nonlinear Phenomena*, 440:133454.

Paszke, A., Gross, S., Massa, F., Lerer, A., Bradbury, J., Chanan, G., Killeen, T., Lin, Z., Gimelshein, N., Antiga, L., Desmaison, A., Kopf, A., Yang, E., DeVito, Z., Raison, M., Tejani, A., Chilamkurthy, S., Steiner, B., Fang, L., Bai, J., and Chintala, S. (2019). Pytorch: An imperative style, high-performance deep learning library. In *Advances in Neural Information Processing Systems 32*, pages 8024–8035. Curran Associates, Inc.

Raissi, M., Perdikaris, P., and Karniadakis, G. (2019). Physics-informed neural networks: A deep learning framework for solving forward and inverse problems involving nonlinear partial differential equations. *Journal of Computational Physics*, 378:686–707.

Salzmann, T., Kaufmann, E., Pavone, M., Scaramuzza, D., and Ryll, M. (2022). Neural-mpc: Deep learning model predictive control for quadrotors and agile robotic platforms. *arXiv preprint arXiv:2203.07747.*

Schiassi, E., Furfaro, R., Leake, C., De Florio, M., Johnston, H., and Mortari, D. (2021). Extreme theory of functional connections: A fast physics-informed neural network method for solving ordinary and partial differential equations. *Neurocomputing*, 457:334–356.

Schoukens, J. and Ljung, L. (2019). Nonlinear system identification: A user-oriented road map. *IEEE Control Systems Magazine*, 39(6):28–99.

Seitzer, M., Tavakoli, A., Antic, D., and Martius, G. (2022). On the pitfalls of heteroscedastic uncertainty estimation with probabilistic neural networks. *arXiv preprint arXiv:2203.09168.*

Spielberg, N. A., Brown, M., and Gerdes, J. C. (2022). Neural network model predictive motion control applied to automated driving with unknown friction. *IEEE Transactions on Control Systems Technology*, 30(5):1934–1945.

Streit, R. L. and Luginbuhl, T. E. (1994). Maximum likelihood training of probabilistic neural networks. *IEEE Transactions on neural networks*, 5(5):764–783.

Wächter, A. and Biegler, L. T. (2006). On the implementation of an interior-point filter line-search algorithm for large-scale nonlinear programming. *Mathematical programming*, 106(1):25:57.

Willems, J., Hostens, E., Depraetere, B., Steinhauser, A., and Swevers, J. (2018). Learning control in practice: Novel paradigms for industrial applications. In *IEEE Conference on Control Technology and Applications (CCTA).*

Yang, L., Meng, X., and Karniadakis, G. E. (2021). B-pinns: Bayesian physics-informed neural networks for forward and inverse pde problems with noisy data. *Journal of Computational Physics*, 425:109913.